Bell *et al. Respiratory Research* (2024) 25:106
https://doi.org/10.1186/s12931-024-02729-x

Respiratory Research

RESEARCH Open Access

Local heterogeneity of normal lung parenchyma and small airways disease are associated with COPD severity and progression

Alexander J. Bell[1], Ravi Pal[1], Wassim W. Labaki[2], Benjamin A. Hoff[1], Jennifer M. Wang[2], Susan Murray[3], Ella A. Kazerooni[1,2], Stefanie Galban[1], David A. Lynch[4], Stephen M. Humphries[4], Fernando J. Martinez[5], Charles R. Hatt[6], MeiLan K. Han[2], Sundaresh Ram[1,7*†] and Craig J. Galban[1,7*†]

Abstract

Background Small airways disease (SAD) is a major cause of airflow obstruction in COPD patients and has been identified as a precursor to emphysema. Although the amount of SAD in the lungs can be quantified using our Parametric Response Mapping (PRM) approach, the full breadth of this readout as a measure of emphysema and COPD progression has yet to be explored. We evaluated topological features of PRM-derived normal parenchyma and SAD as surrogates of emphysema and predictors of spirometric decline.

Methods PRM metrics of normal lung (PRM^{Norm}) and functional SAD (PRM^{fSAD}) were generated from CT scans collected as part of the COPDGene study (n = 8956). Volume density (V) and Euler-Poincaré Characteristic (χ) image maps, measures of the extent and coalescence of pocket formations (i.e., topologies), respectively, were determined for both PRM^{Norm} and PRM^{fSAD}. Association with COPD severity, emphysema, and spirometric measures were assessed via multivariable regression models. Readouts were evaluated as inputs for predicting FEV_1 decline using a machine learning model.

Results Multivariable cross-sectional analysis of COPD subjects showed that V and χ measures for PRM^{fSAD} and PRM^{Norm} were independently associated with the amount of emphysema. Readouts χ^{fSAD} (β of 0.106, $p < 0.001$) and V^{fSAD} (β of 0.065, $p = 0.004$) were also independently associated with FEV_1% predicted. The machine learning model using PRM topologies as inputs predicted FEV_1 decline over five years with an AUC of 0.69.

Conclusions We demonstrated that V and χ of fSAD and Norm have independent value when associated with lung function and emphysema. In addition, we demonstrated that these readouts are predictive of spirometric decline

†Sundaresh Ram and Craig J. Galban are co-last authors.

*Correspondence:
Sundaresh Ram
sundarer@umich.edu
Craig J. Galban
cgalban@med.umich.edu

Full list of author information is available at the end of the article

when used as inputs in a ML model. Our topological PRM approach using PRM^{fSAD} and PRM^{Norm} may show promise as an early indicator of emphysema onset and COPD progression.

Keywords Chronic obstructive pulmonary disease, Small airways disease, Parametric response mapping, Computed tomography of the chest, Machine learning, Emphysema

Background

Chronic obstructive pulmonary disease (COPD) is a leading cause of death and healthcare burden in the United States and worldwide. Accounting for over 3 million deaths globally in 2015 [1], this disease is expected to rise in prevalence as the world population ages [2]. COPD is understood to be a complex heterogeneous disease presenting clinically diverse phenotypes [3, 4]. Major causes of airflow obstruction are attributed to chronic bronchiolar obstruction, a.k.a small airways disease (SAD), and emphysema. Although SAD and emphysema are treated as separate COPD subtypes, studies have shown strong quantitative evidence that SAD exists as an intermediate state between healthy lung tissue and emphysema—i.e., irreversible lung damage—in COPD pathogenesis [5–7]. At present, little has been done to better quantify the onset of SAD from healthy lung parenchyma.

The Parametric Response Map (PRM) is a CT-based voxel-wise computational technique that can identify and quantify functional small airways disease (fSAD; an indirect measure of SAD) even in the presence of emphysema [8]. The percent volume of PRM-derived fSAD (PRM^{fSAD}), i.e., the amount of fSAD in the lungs, has improved COPD phenotyping and the prediction of spirometric decline in subjects at risk of COPD [9]. To determine the value of spatial features from each PRM classification, we developed topological PRM (tPRM) as an extension of the PRM algorithm [10]. These radiographic tPRM readouts were shown to improve upon commonly used whole-lung PRM measures with respect to COPD characterization and progression [11, 12], and correlate to structural changes in lung tissue samples from lung transplant recipients diagnosed with bronchiolitis obliterans [13, 14].

In this study, we evaluated the PRM topologies volume density (V), a measure of extent, and Euler-Poincaré Characteristic (χ), a measure of pocket formation, of normal lung and fSAD as independent readouts of COPD severity, pulmonary function, and extent of emphysema using the Phase 1 COPDGene cohort [15]. We also investigated the potential of these topologic readouts as predictors of spirometric decline using a machine-learning model. This study demonstrates how tPRM readouts may be used as possible measures of early emphysema and COPD progression.

Methods

Study sample

Our study was a secondary analysis of data from COPDGene (ClinicalTrials.gov: NCT00608764), a large Health Insurance Portability and Accountability Act-compliant prospective multi-center observational study. In Phase 1 (2007–2012) and Phase 2 (2013–2017), 5-year follow-up, written and informed consent was obtained from all participants and the study was approved by local institutional review boards of all 21 centers. Ever-smokers with greater than or equal to 10 pack-year smoking history, with and without airflow obstruction, were enrolled between January 2008 and June 2011. Participants were non-Hispanic white or African American. Participants underwent volumetric inspiratory and expiratory CT using standardized protocol; images were transferred to a central lab for protocol verification and quality control (QC) [15]. Exclusion criteria included a history of other lung disease (except asthma), prior surgical excision involving a lung lobe or greater, present cancer, metal in the chest, or history of chest radiation therapy. Participants were excluded from the present study due to inadequate CT for computing tPRM, such as missing an inspiration/expiration scan, or failing QC implemented specifically for the present study. Our QC protocol is described in Additional File 1 (Supplemental Methods 1). Data for participants evaluated here have been utilized in numerous previous studies and a list of COPDGene publications can be found at [16]. Our study is the first to report tPRM analysis across the whole Phase 1 cohort and predict spirometric decline over 5 years in the Phase 2 subset of COPDGene participants.

Spirometry was performed in the COPDGene study before and after the administration of a bronchodilator, specifically 180 mcg of albuterol (Easy-One spirometer; NDD, Andover, MA). Post-bronchodilator values were used in our analyses. COPD was defined by a post-bronchodilator FEV_1/FVC of less than 0.7 at the baseline visit, as specified in the Global Initiative for Chronic Obstructive Lung Disease (GOLD) guidelines [17]. GOLD grades 1–4 were used to define disease severity. GOLD 0 classification, i.e., "at-risk," was defined by a post-bronchodilator $FEV_1/FVC \geq 0.7$ at the baseline visit, alongside FEV_1% predicted ≥ 80%. Participants with $FEV_1/FVC \geq 0.7$ with FEV_1% predicted < 80% were classified as having preserved ratio impaired spirometry (PRISm) [18]. Demographic and spirometric measures used in this study included age, sex, race, smoking history, scanner

manufacturer, body mass index (BMI), FEV_1% predicted, FEV_1/FVC and forced mid-expiratory flow (FEF_{25-75}).

Computed tomography and Topological PRM Analysis

All computed tomography (CT) data were obtained from multiple sites associated with the COPDGene project at Phase 1. Whole-lung volumetric multidetector CT acquisition was performed at full inspiration and normal expiration at functional residual capacity using a standardized previously published protocol [15]. Data reconstructed with the standard reconstruction kernel were used for quantitative analysis. All CT data were presented in Hounsfield units (HU), where stability of CT measurement for each scanner was monitored monthly using a custom COPDGene phantom [15]. For reference, air and water attenuation values are −1,000 and 0 HU, respectively.

PRM were determined from paired CT scans using Lung Density Analysis (LDA) software (Imbio, LLC, Minneapolis, MN). LDA segmented the lungs from the thoracic cavity with airways removed. Inspiratory CT scans were spatially aligned to the expiratory geometric frame using deformable image registration. Lung voxels were classified using pre-determined HU thresholds as: normal (PRM^{Norm}, -950<inspiration HU ≤ -810, and expiration HU ≥ -856), functional small airways disease (PRM^{fSAD}, -950<inspiration HU ≤ -810, expiration HU < -856), emphysema (PRM^{Emph}, inspiration HU < -950, expiration HU < -856), or parenchymal disease (PRM^{PD}, inspiration HU > -810) [19, 20]. Only voxels between −1,000 HU and −250 HU at both inspiration and expiration were used for PRM classification. Each PRM classification was quantified as the percent volume, which is defined as the sum of a PRM classification normalized to the total lung volume at expiration multiplied by 100. There were a few noisy voxels that were considered indeterminate by PRM (inspiration < -950 HU, expiration > -856 HU) that were excluded from our analysis as they did not form consolidated regions of interest within the parenchyma.

Topological analysis of PRM was performed using methods previously described [10]. tPRM metrics were defined through application of Minkowski measures on 3D binary voxel distributions: volume density (V) and Euler-Poincaré Characteristic (χ) [21]. Maps of V and χ were computed for each PRM class (Norm, fSAD, Emph, and PD) using a 3D moving window of size 21×21×21 voxels evaluated on a grid of every 5th voxel. V was normalized by the Minkowski estimate of the mask within the same local window volume (rather than a direct calculation of the mask volume in the window as previously described) and χ by the masked window voxel count. Linear interpolation was applied to determine V and χ values for all segmented voxels.

To indicate the PRM class associated with a Minkowski measure, the class is presented as a superscript (e.g., V^{fSAD} is the volume density of PRM^{fSAD}). tPRM analysis was performed using open-source and in-house software developed in MATLAB R2019a (MATLAB, The MathWorks Inc., Natick, MA). A detailed overview and diagram, of computing tPRM from raw imaging data, was made by Hoff et al. [10]. Because the focus of this study is the relationship between normal parenchyma and SAD, and its association with emphysema, all analyses were performed using V and χ for PRM classifications Norm and fSAD. For completeness, V and χ for PRM classifications Emph and PD are provided.

Phase 1 data and statistical analysis

Data in this study are presented as mean and standard deviation unless stated otherwise. Correlations between V and χ for PRM^{Norm} and PRM^{fSAD} were calculated using Spearman rank-order correlation coefficients (ρ). The total Phase 1 cohort was separated into two subsets based on spirometry-confirmed COPD: non-COPD (FEV_1/FVC≥0.7) and COPD (FEV_1/FVC<0.7). Cross-sectional multivariable regression analysis was performed on both subsets using a stepwise approach with V and χ for PRM classifications Norm and fSAD as independent variables and selected pulmonary function testing and clinical features as outcome variables, controlling for age, gender, race, BMI, smoking (pack years) and CT vendor. These control variables were included as compulsory independent variables in all regression models. Statistical work was conducted using IBM SPSS Statistics v27 (SPSS Software Products). In all tests, significance was defined by $p<0.05$.

Predict spirometric decline

We evaluated baseline V and χ for PRM classifications Norm and fSAD as predictors of FEV_1 decline over 5 years using a machine learning (ML) model. A total of 4483 cases from the Phase 2 cohort of the COPDGene longitudinal trial, a subset of Phase 1, had FEV_1 measurements at baseline and 5-year follow up. Our ML model is a sparse dictionary learning algorithm [22–26] that classifies image patch features as "normal" or "abnormal". In our method, we used the tPRM maps V^{Norm}, V^{fSAD}, χ^{Norm}, and χ^{fSAD} of each case as inputs for training and testing the algorithm. For training our ML model, individual cases were stratified based on the change in FEV_1 over 5 years [= (FEV_1 at yr 5 – FEV_1 at yr 0)/5 years] as fast (ΔFEV_1/yr ≤ -60 ml/yr; n=1516) and slow progressors (ΔFEV_1/yr > -60 ml/yr; n=2967). We used 35% of the data for training and 65% for testing the model [27, 28]. Training was performed on a randomly selected subset of 1569 cases, with n=531 fast progressors and n=1038 slow progressors. The remaining 2914 cases, consisting

of n=985 fast progressors and n=1929 slow progressors, were used for testing the algorithm. In brief, our ML model is designed to associate unique features from the input image patches with fast and slow progressors. This is achieved by randomly selecting image patches from within the lung and extracting the information from the inputs (tPRM maps V^{Norm}, V^{fSAD}, χ^{Norm}, and χ^{fSAD} given as inputs to the ML algorithm) at these image patch locations and comparing their underlying patch features with the compiled class dictionaries of features, which are determined during training. It is important to note that no previous knowledge about the case and lung tissue features, such as emphysema, are provided for the algorithm to delineate "normal" from "abnormal" lung tissue. Details on model design and methods for training and testing are provided in Additional File 1 (Supplemental Fig. 1 and Supplemental Methods 2). To determine the contribution of each feature to the model selection, we used the minimum redundancy maximum relevance feature selection algorithm [29] to rank the tPRM inputs used in the dictionary learning algorithm. The algorithm quantifies the redundancy and relevance using mutual information of variables [30, 31]. We also investigated the selection bias for each input in the ML model and obtained the prediction accuracy for 10 different choices of training image patches, considering each input separately in the model. The prediction accuracy for each training run is fit to a Gaussian probability density function [32, 33]. All processing and analyses were performed using in-house algorithms developed in MATLAB version 2020a (MathWorks, Natick, MA). To determine the contribution of our ML model to account for spatial features in predicting FEV_1 decline, we determined if whole lung mean values of V^{Norm}, V^{fSAD}, χ^{Norm}, and χ^{fSAD} were predictive of FEV_1 decline using a logistic regression classifier.

Case Study: spatial analysis

To better understand the relationship between PRM^{fSAD} and PRM^{Emph}, we evaluated the spatial dependance of V and χ for these PRM classifications from a single subject. The case is a female subject, 48 years of age, diagnosed with GOLD 4 COPD. On a single axial slice, profiles of V and χ for PRM^{fSAD} and PRM^{Emph} were generated by selecting points from high emphysema ($V^{Emph} > 0.6$) and low emphysema ($V^{Emph} < 0.2$). A line plot (Additional File 1: Supplemental Fig. 4) was produced for V and χ vs. distance along each point of the profile. The distance, in units of centimeters, along the image profile was determined using the voxel dimensions of the CT scan. All processing and analyses were performed using in-house algorithms developed in MATLAB version 2020a (MathWorks, Natick, MA).

Results

Population characteristics

The original COPDGene Phase 1 cohort consisted of 10,300 individuals. We excluded 1,344 participants for: inadequate CT data, such as missing an expiration or inspiration scan, to conduct tPRM analysis (n=1,125); missing clinical data (n=16); or failing to pass our CT-based QC testing (n=203). Further details of CT QC are provided in Additional File 1 (Supplemental Methods 1). The resulting complete subset used for analyses thus consisted of 8,956 participants. Baseline demographics and lung function for all Phase 1 participants, grouped based on FEV_1% predicted and FEV_1/FVC—that is, by GOLD grade or PRISm as described in the Methods—are reported in Table 1. Due to the COPDGene recruitment

Table 1 Clinical characterization of the study population

	Non-COPD		COPD			
Variable	**GOLD 0**	**PRISm**	**GOLD 1**	**GOLD 2**	**GOLD 3**	**GOLD 4**
Participants (N)	3867	1088	699	1732	1041	529
Age (yrs)	56.7 (8.36)	57.1 (8.20)	61.6 (8.96)	62.6 (8.86)	64.3 (8.27)	64.1 (7.53)
Sex (M/F)	2048/1819	496/592	399/300	933/799	604/437	314/215
BMI (kg/cm^2)	29.0 (5.79)	31.9 (7.31)	27.1 (4.89)	28.7 (6.06)	28.1 (6.33)	25.3 (5.56)
Smoking (Pack-Years)	37.2 (20.0)	42.6 (24.2)	45.0 (24.4)	50.9 (26.8)	55.1 (27.1)	56.7 (28.7)
FEV_1% Predicted (%)	97.4 (11.4)	70.6 (7.89)	90.8 (8.70)	65.0 (8.51)	40.2 (5.69)	22.6 (4.84)
FEV_1/FVC	0.79 (0.05)	0.77 (0.05)	0.65 (0.04)	0.58 (0.08)	0.44 (0.09)	0.31 (0.07)
FEF_{25-75}(L/s)	2.81 (1.00)	1.79 (0.66)	1.31 (0.50)	0.80 (0.35)	0.39 (0.16)	0.21 (0.08)
PRM^{Norm}(%)	61.7 (13.0)	53.8 (14.6)	56.9 (12.1)	49.1 (13.5)	33.0 (12.5)	21.1 (9.13)
PRM^{fSAD}(%)	9.90 (9.31)	8.88 (8.25)	17.0 (10.8)	21.3 (11.5)	30.9 (11.0)	36.0 (8.94)
PRM^{Emph}(%)	0.80 (1.42)	0.73 (2.29)	3.00 (3.49)	5.40 (6.95)	14.7 (12.2)	26.0 (14.0)
PRM^{PD}(%)	26.3 (12.8)	35.8 (16.4)	20.8 (8.44)	22.2 (9.04)	19.6 (9.29)	15.7 (5.43)

Notes Participant characteristics of the entire study population separated in subsets of those with (FEV_1/FVC<0.7) and without (FEV_1/FVC≥0.7) COPD. Values are displayed as mean (standard deviation). GOLD, Global Initiative for Chronic Obstructive Lung Disease; PRISm, preserved ratio impaired spirometry; GOLD 0, at-risk smokers with normal spirometry; BMI, body mass index; FEV_1, forced expiratory volume in one second; FVC, forced vital capacity; FEF_{25-75}, forced mid-expiratory flow; PRM, parametric response map; Norm, Normal; fSAD, functional small airways disease; Emph, emphysema; PD, parenchymal disease

strategy, the proportion of GOLD 0 ($FEV_1/FVC \geq 0.7$, FEV_1% predicted ≥ 80%) participants [15] account for almost half of the study population (43%; 3,867 of 8,956 participants). Increasing percent volume of PRM-derived fSAD (PRM^{fSAD}) and PRM-derived emphysema (PRM^{Emph}), with decreasing PRM^{Norm}, was observed with higher GOLD grades. This is consistent with previously published work. PRM-derived parenchymal disease (PRM^{PD}) was found to be elevated in PRISm and GOLD 0 participants (35.8 ± 16.4% and 26.3 ± 12.8% of the total lung volume, respectively) as compared to the COPD subset.

Topological readouts of PRM

Presented in Fig. 1 is a case with elevated fSAD (PRM^{fSAD} = 40%). Representative coronal slices of the expiration CT scan and PRM^{fSAD}, overlaid on CT scan, are provided. To illustrate the dependence of χ on the arrangement of PRM^{fSAD}, we have included V^{fSAD} and χ^{fSAD} maps indicating regions with similar values of V^{fSAD} (blue and magenta boxes). As expected, V^{fSAD} (Fig. 1C) is dependent on the amount of fSAD (yellow voxels in Fig. 1B). Averaged over the lungs, V^{fSAD} is proportional to the percent volume of PRM^{fSAD} by a factor of 100. However, $\chi^{fSAD} > 0$ (magenta box in Fig. 1D) corresponds to the formation of fSAD pockets (magenta box Fig. 1B), whereas $\chi^{fSAD} < 0$ (blue box in Fig. 1D) is the consolidation of these pockets into a mesh with holes (blue box in Fig. 1B).

The volume density of PRM^{Norm} and PRM^{fSAD} demonstrated an inverse relationship with increasing COPD severity (Fig. 2A), consistent with previous work. A similar inverse relationship was observed for χ of both normal lung and fSAD (χ^{Norm} and χ^{fSAD}). Values of χ^{Norm} and χ^{fSAD} were found to flip about zero (e.g., χ^{fSAD} changes from positive to negative values) from GOLD 2 to GOLD 4 (Fig. 2B). From Fig. 2B we observe that χ^{Norm} and χ^{fSAD} had means (standard deviations) of -0.0084 (0.0071) and 0.0047 (0.0074), respectively, for cases diagnosed

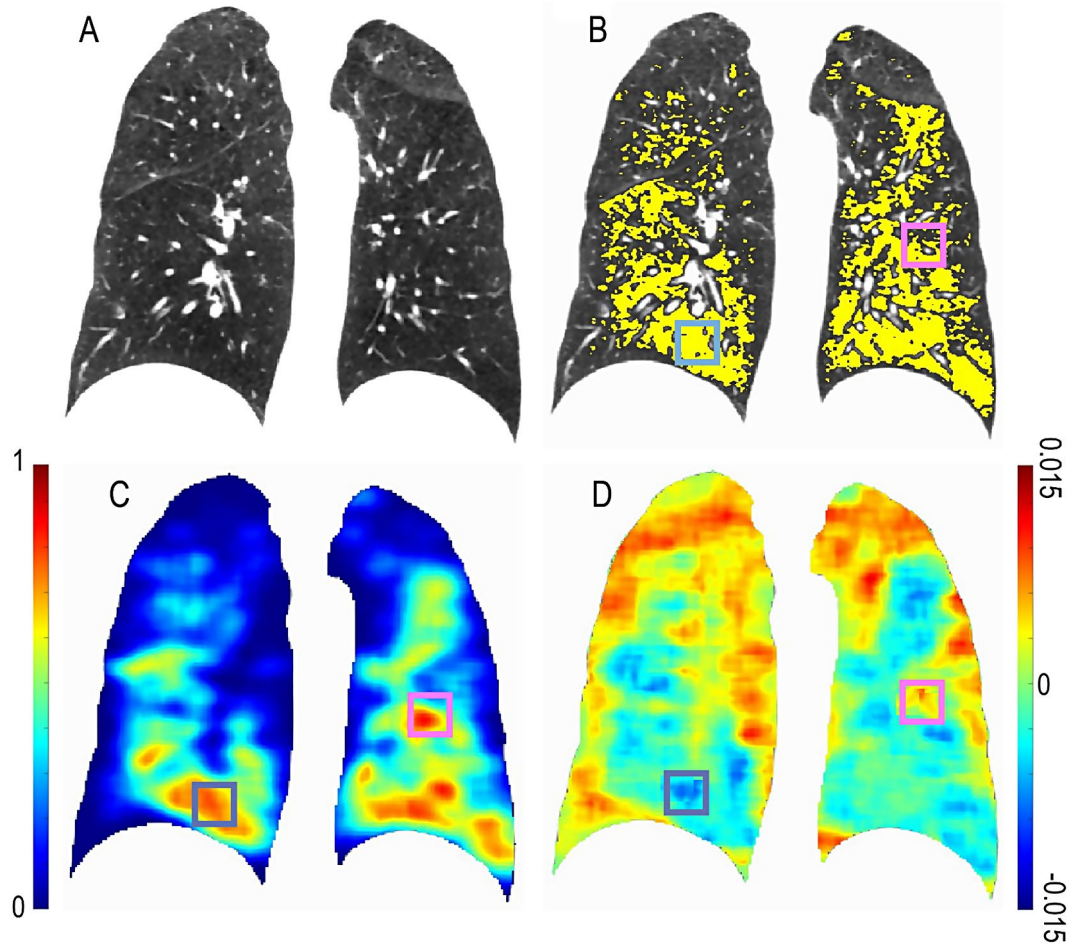

Fig. 1 Illustration of Volume Density (V) and Euler-Poincaré Characteristic (χ) for PRM^{fSAD}. Presented are representative coronal slices for the (**A**) expiratory CT scan with associated (**B**) PRM^{fSAD} overlay (yellow). Included are the (**C**) volume density and (**D**) Euler-Poincaré Characteristic of PRM^{fSAD}. Blue and Magenta boxes indicate two lung regions with elevated V^{fSAD} that have negative and positive χ^{fSAD}, respectively. The subject is a GOLD 3 female aged 53 with FEV_1% predicted of 32% and percent volume of PRM^{fSAD} of 40%

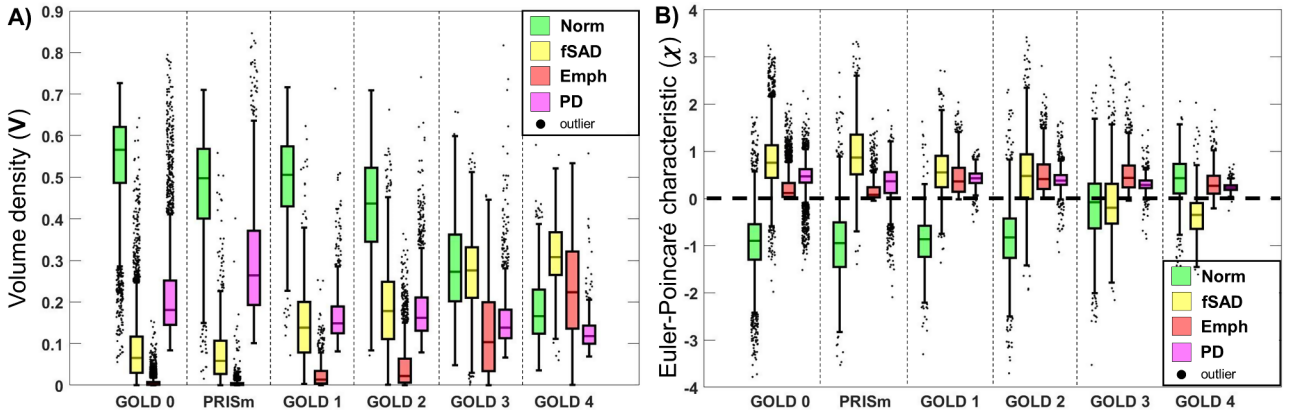

Fig. 2 Boxplots for topological measures of PRM maps PRM^{Norm} (green), PRM^{fSAD} (yellow), PRM^{Emph} (red) and PRM^{PD} (magenta) across all GOLD stages, "at-risk" (GOLD 0), and PRISm. Plots of (**A**) volume density, describing class magnitude (relative amounts of voxels) and (**B**) Euler-Poincaré characteristic, describing class homology, determined by number and type of holes within class volumes. Box plots were computed following standard protocol for box and whiskers; box lines determined by lower quartile (Q1), middle quartile / median (Q2) and upper quartile (Q3), and whiskers are drawn out to Q1−1.5 x IQR and Q3 + 1.5 x IQR for lower and upper limits, respectively. IQR = Q3-Q1. Outliers are defined as points beyond the given upper and lower limits and illustrated as black points with a random bounded horizontal perturbation beyond box whiskers

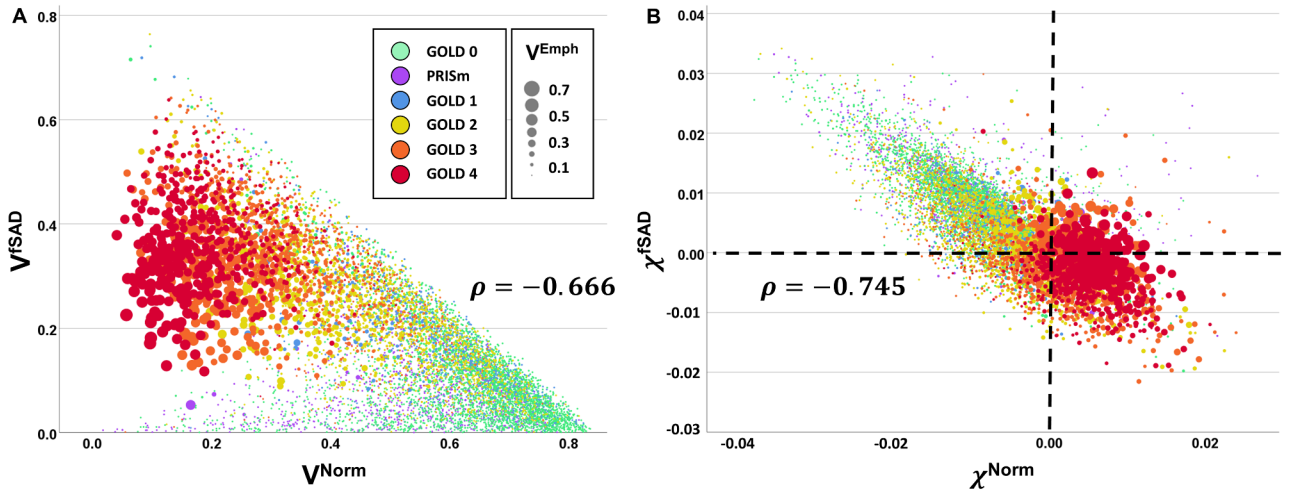

Fig. 3 Scatter plots of all study sample participants for (**A**) V^{Norm} versus V^{fSAD} and (**B**) χ^{Norm} versus χ^{fSAD}. Individual points are color coded based on COPD classifications. The size of the points indicates the amount of emphysema as measured by the volume density of PRM^{Emph} (V^{Emph})

as GOLD 2. For those with severe COPD, i.e., GOLD 4, χ^{Norm} and χ^{fSAD} are 0.0039 (0.0055) and −0.0036 (0.0048), respectively. Mean values of χ^{Emph} and χ^{PD} were found to be positive and similar across GOLD. We did not consider mean breadth and surface area of PRM^{Norm} and PRM^{fSAD} in our analysis, as we did not see such a strong relationship between them (Additional File 1: Supplementary Fig. 2).

We further evaluated the relationship of PRM^{Norm} and PRM^{fSAD} with respect to V (Fig. 3A) and χ (Fig. 3B). Both V and χ demonstrated strong correlations between Norm and fSAD (ρ = -0.666, $p<0.001$ and ρ = -0.745, $p<0.001$, respectively) over the Phase 1 cohort. Here the GOLD stages are coded by color and the relative amount of emphysema, quantified by V^{Emph}, by size of the marker. As observed in Fig. 3A, V^{Norm} versus V^{fSAD} had more scatter in the data compared to χ^{Norm} versus χ^{fSAD} (Fig. 3B). As expected, GOLD 4 cases with elevated emphysema (V^{Emph}) demonstrated a drop in V^{Norm} and V^{fSAD} values. In contrast, χ^{Norm} consisted of primarily positive values, whereas positive and negative values were observed for χ^{fSAD} (Fig. 3B). Although V^{fSAD} was found to be strongly correlated to V^{Emph} (ρ=0.845, $p<0.001$), only a weak correlation was observed between χ^{fSAD} and χ^{Emph} (ρ = -0.155, $p<0.001$).

Multivariable regression analysis

Presented in Table 2 are results from multivariable regression analyses that demonstrate the contribution of V and χ to PRM^{Norm} and PRM^{fSAD} when modeling spirometric measures and the volume density of emphysema, controlling for age, sex, race, BMI, pack-years,

Table 2 Multivariable regression for COPD subset

Performance	FEV_1% predicted	FEV_1/FVC	FEF_{25-75} (L)	V^{Emph}
Adjusted R^2	0.516	0.602	0.526	0.778
SE	15.8	0.084	0.331	0.057
Age (yrs)	0.085**	0.021 (0.06)	-0.184**	0.035**
Sex (M/F)		0.018 (0.08)	-0.283**	-0.035**
BMI (kg/cm^2)	-0.110**	0.033*	0.024**	-0.232**
Smoking (Pack Years)	-0.046**	-0.013 (0.22)	-0.051**	-0.015 (0.06)
CT vendor				0.111**
Race		0.113**	-0.033*	
V^{Norm}	0.727**	0.668**	0.688**	-1.01**
V^{fSAD}	0.065*		0.138**	-0.408**
χ^{Norm}		-0.120**	0.134**	0.150**
χ^{fSAD}	0.106**		0.175**	0.118**

Notes Multivariable regression modelling using volume density (V) and Euler-Poincaré Characteristic (χ) for PRM-derived Normal and fSAD (introduced stepwise) to model pulmonary function testing measures in the COPD subset. Each column presents results for a different regression model. FEV_1, forced expiratory volume in one second; FVC, forced vital capacity; FEF_{25-75}, forced mid-expiratory flow; Emph, emphysema; SE, standard error of the estimate; BMI, body mass index; Norm, Normal; fSAD, functional small airways disease. Model performance is reported as adjusted R^2 and standard error of the estimate. Feature association is reported as standardized beta coefficients (β); cells for stepwise variables removed from final model. All regression models were controlled for age, sex, race, BMI, pack years and CT vendor. P values ≥ 0.01, < 0.01 and ≥ 0.001, and < 0.001 are presented as values in parentheses, *, and **, respectively

and CT vendor. Among those with spirometrically confirmed COPD, V^{Norm} was found to be significantly associated with multiple clinical measures including FEV_1% predicted, FEV_1/FVC, FEF_{25-75} and V^{Emph} (see Table 2). V^{fSAD} and χ^{fSAD} were found to independently and significantly contribute to FEV_1% predicted (β=0.065, p=0.004 and β=0.106, p<0.001). Only the Norm topological measures were found to contribute to FEV_1/FVC (β=0.668, p<0.001 for V^{Norm} and β = -0.120, p<0.001 for χ^{Norm}), whereas V and χ for both Norm and fSAD were found to be significant parameters for FEF_{25-75}. With respect to V^{Emph}, extent of emphysema, V and χ for Norm and fSAD were highly significant but demonstrated similar trends irrespective of PRM classification. For completeness, the same analyses were performed on the non-COPD cohort (Additional File 1: Supplemental Table 1). As compared to the COPD cohort, statistical models generated from the non-COPD cohort demonstrated significant parameters but with weaker correlations (i.e., adjusted R^2).

Prediction model of spirometric decline

Representative axial slices of expiration CT scan, PRM, V^{fSAD}, χ^{fSAD} and corresponding patch probability maps from a fast progressor (with ΔFEV_1/yr of -249 ml/yr) are provided in Fig. 4. Our ML model correctly classified this subject as a fast progressor. This case is a 63-year-old male, diagnosed at baseline with GOLD 2 COPD. Using V and χ from PRM^{fSAD} and PRM^{Norm} as inputs, the ML model was able to determine regions of emphysema, discernible from existing fSAD, observed in the right upper lung as "abnormal" (blue patches in the probability maps). In contrast, the dorsal lung regions were classified as "normal" (red patches in the probability maps) due to the absence of fSAD and emphysema. For completeness we have provided in Additional File 1 (Supplemental Fig. 3) representative axial slices of expiration CT scan, PRM, V^{fSAD}, χ^{fSAD} and corresponding patch probability maps from a slow progressor (with ΔFEV_1/yr of 101 ml/yr).

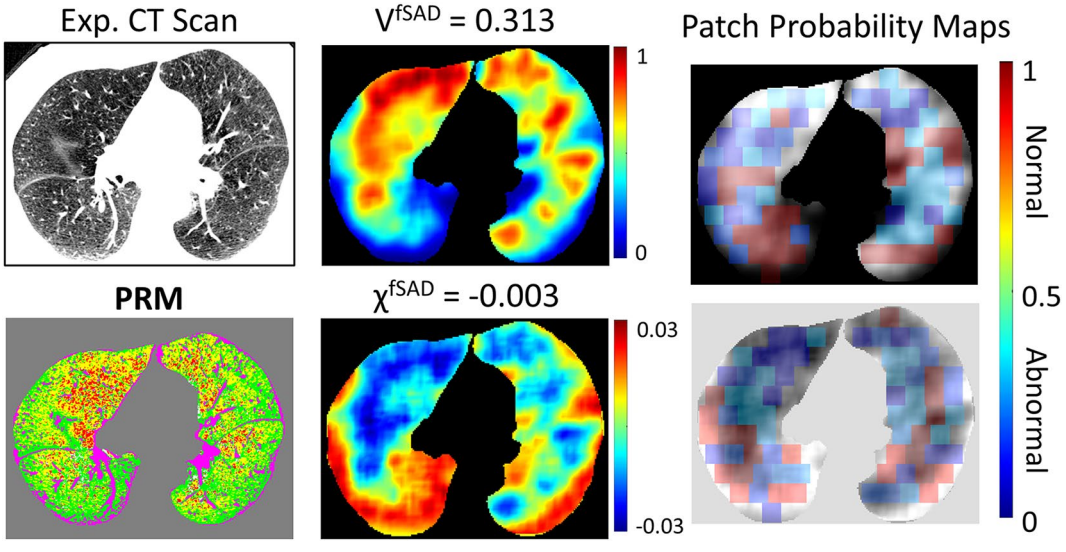

Fig. 4 The dictionary learning results for a 63-year-old male diagnosed at baseline with GOLD 2 COPD and declared a fast progressor with ΔFEV_1/yr of -249 ml/yr. Representative axial slice of an expiratory CT scan acquired at baseline, its associated PRM map, the tPRM maps V^{fSAD} and χ^{fSAD} of PRM^{fSAD}, and their image patch probability maps from the dictionary learning model

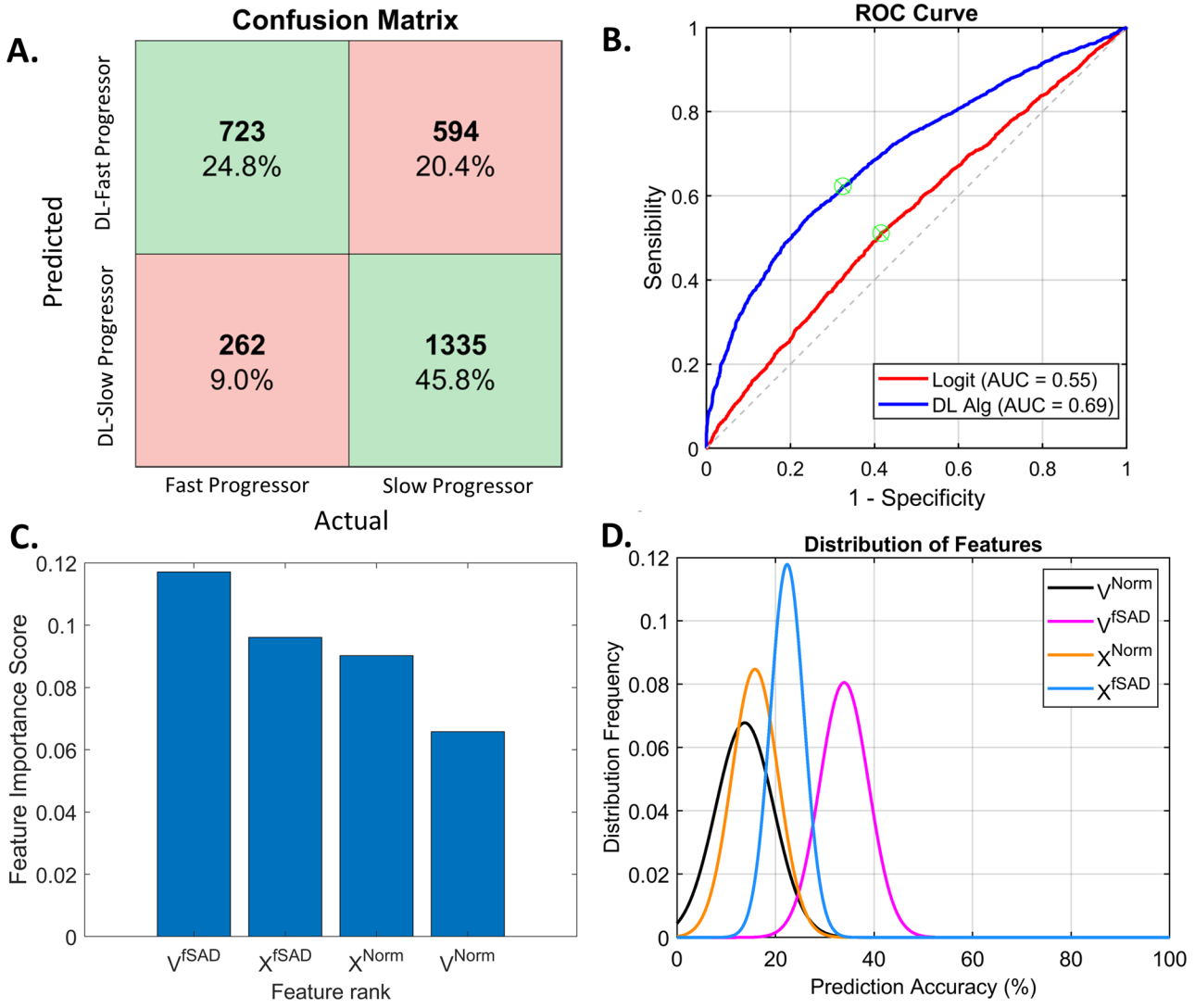

Fig. 5 Results and relevance of the different features (tPRM metrics as inputs) used in the dictionary learning method. (**A**) Confusion Matrix showing the sensitivity and specificity of the ML model classifications for both the fast progressor (n = 985) and the slow progressor (n = 1929) classes in the test set. Green colored and red colored fields in the matrix represent agreement and disagreement, respectively, of the ML model with the actual decision. (**B**) Receiver Operating Characteristic (ROC) curve for our ML model and the logistic regression classifier with the corresponding Area Under the Curve (AUC) statistics. (**C**) Bar plot showing the feature importance score and feature ranking using the minimum redundancy maximum relevance method. (**D**) Plot showing the distribution of the features and their prediction accuracy over ten different training runs

As seen in Fig. 5A and B, our ML model had an overall classification accuracy of 70.6% and Area Under the Curve (AUC) of 0.69 of the receiver operating characteristic (ROC) curve. We compared our ML model with a simple logistic regression model using whole lung mean values of V^{Norm}, V^{fSAD}, χ^{Norm}, and χ^{fSAD}. Figure 5B shows that the logistic regression model only achieved an AUC of 0.55. The contribution of each of the inputs to the model (V^{Norm}, V^{fSAD}, χ^{Norm}, and χ^{fSAD}) are shown in Fig. 5C and D. V and χ of PRM^{fSAD} are dominant inputs, followed by V and χ of PRM^{Norm} (Fig. 5C). Using a feature rank analysis performed on our test set, we observed that V and χ of PRM^{fSAD} are important to achieve higher prediction accuracy. In fact, χ^{fSAD} was found to have the smallest spread/variance (Fig. 5D), indicating highly desirable robustness to the choice of training image patches and its usefulness as an input in the ML model. As reported in Table 3, "normal" patches, on average, consisted primarily of PRM^{Norm}, elevated V^{Norm} (abundant) and negative χ^{Norm} (consolidated), with negligible

Table 3 Image patch topological PRM metrics in the ML model

tPRM Metrics	Normal	Abnormal
V^{Norm}	0.5458 (0.1587)	0.3798 (0.0897)
V^{fSAD}	0.1059 (0.0935)	0.3299 (0.1008)
χ^{Norm}	-0.0065 (0.0084)	-0.0031 (0.0058)
χ^{fSAD}	0.0041 (0.0061)	-0.0019 (0.0062)

Note Data are presented as the mean (standard deviation)

PRM^{fSAD}, low V^{fSAD} (depleted) and positive χ^{fSAD} (sparse pockets). In "abnormal" patches, similar values of V and χ for PRM^{Norm} and PRM^{fSAD} were observed (Table 3). Positive and negative values in χ^{fSAD} were found for "normal" and "abnormal" patches, respectively. This is consistent with the inverse relationship seen with increasing COPD severity shown in Fig. 2.

Dependence between topologies of PRM^{fSAD} and PRM^{Emph}

As the topologies of PRM were determined as averages over the whole lungs, we provide a case study illustrating the relationship between V and χ of PRM^{fSAD} and PRM^{Emph} at the local level. Presented in Additional File 1 (Supplemental Fig. 4) are the profiles of V and χ of PRM^{fSAD} and PRM^{Emph} from a region of the right lung with elevated and reduced V^{Emph} (orange circle and star, respectively; Supplemental Fig. 4A and C). The case is a female subject, 48 years of age, diagnosed with GOLD 4 COPD. The subject was found to have on average high levels of V^{fSAD} (0.37) with relatively elevated V^{Emph} (0.1). Mean values for the whole lungs of χ were 0.008 and −0.009 for PRM^{Emph} and PRM^{fSAD}, respectively. As seen in Additional File 1 (Supplemental Fig. 4C), V^{fSAD} increased while V^{Emph} decreased further from lung with the highest level of V^{Emph} (~0.6 at orange circle in Additional File 1: Supplemental Fig. 4A and C). At approximately 1.8 cm, volume densities between PRM^{fSAD} and PRM^{Emph} transitioned. In addition, χ^{fSAD} was found to increase with decreasing χ^{Emph} with transition occurring at ~1.2 cm.

Discussion

The topological parametric response map is an extension of the well-established PRM method, a quantitative imaging marker of SAD [8]. In this study, we have demonstrated that inclusion of topological features, in this case the Euler-Poincaré Characteristic (χ), improved characterization and interpretation of fSAD in COPD as a complimentary readout of volume density (V), which is equivalent to traditional percent volume of PRM classifications [10]. This study also evaluated the role of PRM-defined normal parenchyma (PRM^{Norm}) and fSAD (PRM^{fSAD}) as lone indicators of COPD severity. We observed distinct patterns in topological metrics with respect to GOLD grades and identified a complete inversion in topology, characterized by Euler-Poincaré Characteristic χ, between normal lung and fSAD, in mid-to-late stages of COPD. We also found V and χ of PRM^{Norm} and PRM^{fSAD} to have statistically significant correlation with spirometric measures and emphysema and to be predictive of spirometric decline.

Our study builds on previous work by Hoff et al. [10] on tPRM characterization in COPD. This study used a much smaller population (n=88) to demonstrate the trends of all four topological features (volume density, surface area, mean curvature and Euler-Poincaré Characteristic) with increasing COPD severity [10]. Limited in statistical power, it instead focused on the surface area of fSAD. Access to a notably larger population (n=8,956) in the current study allowed us to evaluate the volume density (V) and Euler-Poincaré Characteristic (χ) of PRM^{Norm} and PRM^{fSAD} and relate our findings to the field's current understanding of COPD progression, i.e., normal parenchyma transitions to emphysema through SAD.

A key finding of our study is the ability to quantify parenchymal lung health, based not only on the extent but also on the arrangement of local lung abnormalities, i.e., fSAD. This is rooted in the concept that the lungs are healthy (i.e., PRM^{Norm}) and COPD progresses through SAD (i.e., PRM^{fSAD}), an intermediate between normal and emphysematous lung tissue, to emphysema. The nature of this transition suggests χ may be capturing a fundamental mechanism in the emergence of fSAD. Based on our observation, fSAD appears to develop as distinct pockets, which are represented as positive values in χ^{fSAD} within healthy lung tissue, as depicted in the blue box in Fig. 1B. With increasing COPD severity, fSAD pockets coalesce to a mesh, which is represented by negative values in χ^{fSAD} (magenta box in Fig. 1B). On a whole lung level, this transition occurs on average from GOLD stages 2 to 4. By quantifying the amount and arrangement of normal and fSAD parenchyma, one can assess the severity of COPD. As fSAD is an intermediate between healthy lung and emphysema, increasing levels of emphysema have a direct effect on V and χ of fSAD. This is observed in Fig. 3 and Additional File 1 (Supplemental Fig. 4), where increasing values of V^{Emph} resulted in a drop in V^{fSAD} and increase in χ^{fSAD}. These trends were reflected in our multivariable model for V^{Emph} as well (Table 2).

In a seminal study, McDonough and colleagues [7] provided pathological evidence demonstrating the role of SAD in COPD progression. Using high resolution (~10 μm) microCT to analyze frozen lung samples from lung transplant recipients with end-stage COPD, they found that widespread narrowing and destruction of the smaller airways (i.e., SAD) occurred before emphysematous lesions became large enough to be visible on standard CT imaging. They concluded that SAD might serve as an emphysema precursor. Based on their observation, we postulated that the transition observed between χ^{Norm} and χ^{fSAD} (Figs. 2 and 3) should be observed for χ^{fSAD} and χ^{Emph}. Using mean values of χ over the lungs, χ^{Emph} was found to be relatively stable, generating positive values across GOLD (Additional File 1: Supplemental Fig. 2), as well as demonstrating a weak correlation to χ^{fSAD} ($\rho = -0.155$, $p<0.001$). Nevertheless, evaluating χ^{fSAD} and χ^{Emph} at the local level, we observe a strong association

between these two readouts (Additional File 1: Supplemental Fig. 4), which may be linked to the structural changes in the terminal airways observed using microCT of lung explants.

In a recent study, Bhatt and colleagues evaluated a CT readout, referred to as the mean Jacobian determinant of normal voxels, at varying distances from emphysematous tissue [34]. When measured at 2 mm from CT voxels designated emphysema (i.e., voxel HU <-950 HU), this CT-based readout was found to be predictive of spirometric decline. Our spatial analysis of a single case clearly demonstrates a transition in topologies of PRM^{fSAD} and PRM^{Emph}, 1.8 cm and 1.2 cm for V and χ, respectively (Additional File 1: Supplemental Fig. 4). It is the association of topologies between PRM^{fSAD} and PRM^{Emph} at the local level that allows our machine learning model to predict spirometric decline, with an accuracy of 70%, in the absence of any emphysema readout as an input (Fig. 4). Although the readouts reported by Bhatt and colleagues lacked quantification of SAD, there is clear agreement that lung tissue along the periphery of emphysematous tissue provides potential insight into COPD progression. Using only topologies of PRM^{Norm} and PRM^{fSAD}, our patch-based ML model outperformed the whole-lung logistic regression model (Fig. 5B). This result highlights the importance of the spatial relationship of χ^{fSAD} to χ^{Emph} to predict spirometric decline (Figs. 4 and 5).

We acknowledge several notable limitations. COPDGene comprises over 20 study sites, making scanner variation and reconstruction kernel inconsistency inevitable. Sensitivity of PRM to scanner variability was addressed previously [35] and although effort was made to apply PRM only to soft kernels, variability in scanner type was unavoidable. However, we included scanner vendor in our multivariable regressions and found that it did not significantly confound models. Another limitation is variation in levels of inspiration and expiration during CT acquisition. Earlier work demonstrated that even small perturbations from functional residual capacity (FRC) have an observable effect on threshold-based techniques such as PRM [35]. To limit this, we implemented QC that excluded participants based on erroneous volume changes or strong discordance with correlation between PRM^{Norm} and FEV_1% predicted.

Conclusions

In this paper, we have demonstrated that topological features, V and χ, are able to enhance the sensitivity of PRM classifications, notably Norm and fSAD, to extent of emphysema and COPD severity. These data support the concept that as pockets of small airways disease coalesce, surrounding normal tissue is lost. Pockets of fSAD are seen to correlate with increasing presence of emphysema, independent of the amount of fSAD present. We further demonstrated that local levels of χ^{fSAD} and χ^{Emph} correlate, which may be explained by bronchiolitis along the periphery of emphysematous tissue observed by McDonough and colleagues using microCT. In addition, we demonstrated that local values of V and χ for PRM^{Norm} and PRM^{fSAD} provide sufficient information to predict spirometric decline, even in the absence of any prior knowledge of emphysema. Our study provides a unique strategy to detect subtle changes in lung parenchyma that may progress to emphysema. This approach to monitoring extent and arrangement of Norm and fSAD offers insight into COPD phenotypes and provides improved prognostic information that has relevance in clinical care and future clinical trials.

Abbreviations

BMI	body mass index
COPD	chronic obstructive pulmonary disease
COPDGene	Genetic Epidemiology of Chronic Obstructive Pulmonary Disease
CT	computed tomography
Emph	emphysema
FEF_{25-75}	forced mid-expiratory flow
FEV_1	forced expiratory volume in 1 s
FEV_1%pred, FEV_1pp	FEV_1 percent predicted
FRC	functional residual capacity
fSAD	functional small airways disease
FVC	forced vital capacity
GOLD	Global Initiative for Chronic Obstructive Lung Disease
HU	Hounsfield unit
LDA	Lung Density Analysis (software)
ML	machine learning
Norm	normal lung parenchyma
PD	parenchymal disease
PRISm	preserved ratio impaired spirometry
PRM	Parametric Response Mapping
PRM^{Emph}	amount of emphysema in the lungs, calculated using Parametric Response Mapping
PRM^{fSAD}	amount of functional small airways disease in the lungs, calculated using Parametric Response Mapping
PRM^{Norm}	amount of normal lung, calculated using Parametric Response Mapping
PRM^{PD}	amount of parenchymal disease in the lungs, calculated using Parametric Response Mapping
QC	quality control
ROC	receiver operating characteristic
SAD	small airways disease
SE	standard error of the estimate
tPRM	Topological Parametric Response Mapping
V	volume density
V^{Emph}	volume density of PRM^{Emph}
V^{fSAD}	volume density of PRM^{fSAD}
V^{Norm}	volume density of PRM^{Norm}
χ	Euler-Poincaré Characteristic
χ^{Emph}	Euler-Poincaré Characteristic measure of PRM^{Emph}
χ^{fSAD}	Euler-Poincaré Characteristic measure of PRM^{fSAD}
χ^{Norm}	Euler-Poincaré Characteristic measure of PRM^{Norm}

Supplementary Information

The online version contains supplementary material available at https://doi.org/10.1186/s12931-024-02729-x.

Supplementary Material 1

Acknowledgements
We acknowledge the COPDGene investigators for their role in the study providing data for this project: Administrative Center: James D. Crapo, MD (PI); Edwin K. Silverman, MD, PhD (PI); Barry J. Make, MD; Elizabeth A. Regan, MD, PhD. Genetic Analysis Center: Terri Beaty, PhD; Ferdouse Begum, PhD; Peter J. Castaldi, MD, MSc; Michael Cho, MD; Dawn L. DeMeo, MD, MPH; Adel R. Boueiz, MD; Marilyn G. Foreman, MD, MS; Eitan Halper-Stromberg; Lystra P. Hayden, MD, MMSc; Craig P. Hersh, MD, MPH; Jacqueline Hetmanski, MS, MPH; Brian D. Hobbs, MD; John E. Hokanson, MPH, PhD; Nan Laird, PhD; Christoph Lange, PhD; Sharon M. Lutz, PhD; Merry-Lynn McDonald, PhD; Margaret M. Parker, PhD; Dmitry Prokopenko, Ph.D; Dandi Qiao, PhD; Elizabeth A. Regan, MD, PhD; Phuwanat Sakornsakolpat, MD; Edwin K. Silverman, MD, PhD; Emily S. Wan, MD; Sungho Won, PhD. Imaging Center: Juan Pablo Centeno; Jean-Paul Charbonnier, PhD; Harvey O. Coxson, PhD; Craig J. Galban, PhD; MeiLan K. Han, MD, MS; Eric A. Hoffman, Stephen Humphries, PhD; Francine L. Jacobson, MD, MPH; Philip F. Judy, PhD; Ella A. Kazerooni, MD; Alex Kluiber; David A. Lynch, MB; Pietro Nardelli, PhD; John D. Newell, Jr., MD; Aleena Notary; Andrea Oh, MD; Elizabeth A. Regan, MD, PhD; James C. Ross, PhD; Raul San Jose Estepar, PhD; Joyce Schroeder, MD; Jered Sieren; Berend C. Stoel, PhD; Juerg Tschirren, PhD; Edwin Van Beek, MD, PhD; Bram van Ginneken, PhD; Eva van Rikxoort, PhD; Gonzalo Vegas Sanchez-Ferrero, PhD; Lucas Veitel; George R. Washko, MD; Carla G. Wilson, MS; PFT QA Center, Salt Lake City, UT: Robert Jensen, PhD. Data Coordinating Center and Biostatistics, National Jewish Health, Denver, CO: Douglas Everett, PhD; Jim Crooks, PhD; Katherine Pratte, PhD; Matt Strand, PhD; Carla G. Wilson, MS. Epidemiology Core, University of Colorado Anschutz Medical Campus, Aurora, CO: John E. Hokanson, MPH, PhD; Gregory Kinney, MPH, PhD; Sharon M. Lutz, PhD; Kendra A. Young, PhD. Mortality Adjudication Core: Surya P. Bhatt, MD; Jessica Bon, MD; Alejandro A. Diaz, MD, MPH; MeiLan K. Han, MD, MS; Barry Make, MD; Susan Murray, ScD; Elizabeth Regan, MD; Xavier Soler, MD; Carla G. Wilson, MS. Biomarker Core: Russell P. Bowler, MD, PhD; Katerina Kechris, PhD; Farnoush Banaei-Kashani, Ph.D. We would also like to acknowledge our copy editor Lee Olsen for her assistance in preparing this manuscript.

Author contributions
AJB: conceptualization, methodology, software, validation, formal analysis, data curation, writing – original draft, writing – review & editing, visualization. RP: software, formal analysis, writing – review & editing. WWL: resources, writing – review & editing, supervision. BAH: software, formal analysis, data curation, writing – review & editing. JMW: validation, resources, writing – review & editing. SM: formal analysis, investigation, data curation, writing – review & editing, project administration. EAK: resources, writing – review & editing, supervision, project administration. SG: resources, writing – review & editing, supervision, project administration. DAL: resources, writing – review & editing, supervision, project administration. SMH: resources, writing – review & editing, supervision, project administration. FJM: resources, writing – review & editing, supervision, project administration. CRH: conceptualization, methodology, resources, writing – review & editing, supervision, project administration, funding acquisition. MKH: conceptualization, methodology, resources, writing – review & editing, supervision, project administration, funding acquisition. SR: conceptualization, methodology, software, validation, formal analysis, investigation, data curation, writing - original draft, writing – review & editing, visualization, supervision, project administration. CJG: conceptualization, methodology, software, validation, formal analysis, investigation, resources, data curation, writing – original draft, writing – review & editing, visualization, supervision, project administration, funding acquisition.

Funding
This work was supported by the National Heart, Lung, and Blood Institute of the National Institutes of Health Grants R01 HL139690 (to CJG), R01 HL150023 (to MKH, CJG, and CRH) and T32 HL 007749 (to JMW) and by the National Heart, Lung, and Blood Institute of the National Institutes of Health Grants U01 HL089897 and U01 HL089856 and by NIH contract 75N92023D00011, which support the COPDGene study. The COPDGene study (NCT00608764) has also been supported by the COPD Foundation through contributions made to an Industry Advisory Committee that has included AstraZeneca, Bayer Pharmaceuticals, Boehringer-Ingelheim, Genentech, GlaxoSmithKline, Novartis, Pfizer and Sunovion.

Data availability
The datasets presented in this study are not readily available because they are part of an NIH-sponsored clinical trial and require a data use agreement to be signed. For access to COPDGene data visit https://www.copdgene.org/phase-1-study-documents.htm for instructions.

Declarations

Ethics approval and consent to participate
Our study was a secondary analysis of data from COPDGene (ClinicalTrials.gov: NCT00608764), a large Health Insurance Portability and Accountability Act-compliant prospective multi-center observational study. In Phase 1 (2007–2012) and Phase 2 (2013–2017), 5-year follow-up, written and informed consent was obtained from all participants and the study was approved by local institutional review boards of all 21 centers.

Consent for publication
Our study did not require consent for publication from individuals as it was a secondary analysis of data from COPDGene (ClinicalTrials.gov: NCT00608764). Written and informed consent for the COPDGene study was obtained from all participants and the study was approved by local institutional review boards of all 21 centers. For our study, data from COPDGene was anonymized and our authors had no access to identifying information for COPDGene study participants.

Competing interests
Wassim W. Labaki reports personal fees from Continuing Education Alliance. Benjamin A. Hoff and Craig J. Galban are co-inventors and patent holders of tPRM, which the University of Michigan has licensed to Imbio, LLC. Craig J. Galban is co-inventor and patent holder of PRM, which the University of Michigan has licensed to Imbio, LLC. Benjamin A. Hoff and Craig J. Galban have financial interest in Imbio, LLC. Charles R. Hatt is employed by Imbio, LLC. David A. Lynch reports funds paid to the institution from NIH and personal payments from Boehringer Ingelheim. MeiLan K. Han reports personal fees from GlaxoSmithKline, AstraZeneca, Boehringer Ingelheim, Cipla, Chiesi, Novartis, Pulmonx, Teva, Verona, Merck, Mylan, Sanofi, DevPro, Aerogen, Polarian, Regeneron, Amgen, UpToDate, Altesa Biopharma, Medscape, NACE, MDBriefcase and Integrity. She has received either in kind research support or funds paid to the institution from the NIH, Novartis, Sunovion, Nuvaira, Sanofi, AstraZeneca, Boehringer Ingelheim, Gala Therapeutics, Biodesix, the COPD Foundation and the American Lung Association. She has participated in Data Safety Monitoring Boards for Novartis and Medtronic with funds paid to the institution. She has received stock options from Meissa Vaccines and Altesa Biopharma. For the remaining authors none were declared.

Author details
[1]Department of Radiology, University of Michigan, 109 Zina Pitcher Place BSRB A506, Ann Arbor, MI 48109-2200, USA
[2]Department of Internal Medicine, Division of Pulmonary and Critical Care Medicine, University of Michigan, Ann Arbor, MI, USA
[3]School of Public Health, University of Michigan, Ann Arbor, MI, USA
[4]Department of Radiology, National Jewish Health, Denver, CO, USA
[5]Weill Cornell Medical College, New York, NY, USA
[6]Imbio, LLC, Minneapolis, MN, USA
[7]Department of Biomedical Engineering, University of Michigan, Ann Arbor, MI, USA

Received: 9 January 2024 / Accepted: 13 February 2024
Published online: 28 February 2024

References
1. Global regional. National deaths, prevalence, disability-adjusted life years, and years lived with disability for chronic obstructive pulmonary disease and asthma, 1990–2015: a systematic analysis for the global burden of disease study 2015. Lancet Respiratory Med. 2017;5(9):691–706.
2. Mannino DM, Buist AS. Global burden of COPD: risk factors, prevalence, and future trends. Lancet. 2007;370(9589):765–73.

3. Han MK, Agusti A, Calverley PM, Celli BR, Criner G, Curtis JL, et al. Chronic obstructive pulmonary disease phenotypes. Am J Respir Crit Care Med. 2010;182(5):598–604.
4. Barker BL, Brightling CE. Phenotyping the heterogeneity of chronic obstructive pulmonary disease. Clin Sci (Lond). 2013;124(6):371–87.
5. Boes JL, Hoff BA, Bule M, Johnson TD, Rehemtulla A, Chamberlain R, et al. Parametric response mapping monitors temporal changes on lung CT scans in the subpopulations and intermediate outcome measures in COPD study (SPIROMICS). Acad Radiol. 2015;22(2):186–94.
6. Labaki WW, Gu T, Murray S, Hatt CR, Galban CJ, Ross BD, et al. Voxel-wise longitudinal parametric response mapping analysis of chest computed tomography in smokers. Acad Radiol. 2019;26(2):217–23.
7. McDonough JE, Yuan R, Suzuki M, Seyednejad N, Elliott WM, Sanchez PG, et al. Small-airway obstruction and emphysema in chronic obstructive pulmonary disease. N Engl J Med. 2011;365(17):1567–75.
8. Galbán CJ, Han MK, Boes JL, Chughtai KA, Meyer CR, Johnson TD, et al. Computed tomography–based biomarker provides unique signature for diagnosis of COPD phenotypes and disease progression. Nat Med. 2012;18(11):1711–5.
9. Bhatt SP, Soler X, Wang X, Murray S, Anzueto AR, Beaty TH, et al. Association between functional small airway disease and FEV1 decline in chronic obstructive pulmonary sisease. Am J Respir Crit Care Med. 2016;194(2):178–84.
10. Hoff BA, Pompe E, Galbán S, Postma DS, Lammers J-WJ, ten Hacken NHT, et al. CT-Based local distribution metric improves characterization of COPD. Sci Rep. 2017;7(1):2999.
11. Wang JM, Bell AJ, Ram S, Labaki WW, Hoff BA, Murray S et al. Topologic parametric response mapping identifies tissue subtypes associated with emphysema progression. Acad Radiol. 2023.
12. Wang JM, Bell AJ, Ram S, Labaki WW, Hoff BA, Murray S et al. Topologic parametric response mapping identifies emphysema progression subtypes in COPDGene. D92 Novel imaging and physiologic measures in COPD. American thoracic society international conference abstracts: American Thoracic Society; 2023. p. A6544-A.
13. Ram S, Verleden SE, Bell AJ, Hoff BA, Labaki WW, Murray S, et al. Quantitative CT correlates with local inflammation in lung of patients with subtypes of chronic lung allograft dysfunction. Cells. 2022;11(4):699.
14. Cheng GS, Selwa KE, Hatt C, Ram S, Fortuna AB, Guerriero M, et al. Multicenter evaluation of Parametric response mapping as an indicator of bronchiolitis obliterans syndrome after hematopoietic stem cell transplantation. Am J Transpl. 2020;20(8):2198–205.
15. Regan EA, Hokanson JE, Murphy JR, Make B, Lynch DA, Beaty TH et al. Genetic epidemiology of COPD (COPDGene) study design. COPD: Journal of Chronic Obstructive Pulmonary Disease. 2011;7(1):32–43.
16. Publications Resulting from the COPDGene Project. [Available from: https://www.copdgene.org/publications.htm.
17. Rabe KF, Hurd S, Anzueto A, Barnes PJ, Buist SA, Calverley P, et al. Global strategy for the diagnosis, management, and prevention of chronic obstructive pulmonary disease. Am J Respir Crit Care Med. 2007;176(6):532–55.
18. Wan ES, Castaldi PJ, Cho MH, Hokanson JE, Regan EA, Make BJ, et al. Epidemiology, genetics, and subtyping of preserved ratio impaired spirometry (PRISm) in COPDGene. Respir Res. 2014;15:89.
19. Belloli EA, Degtiar I, Wang X, Yanik GA, Stuckey LJ, Verleden SE, et al. Parametric response mapping as an imaging biomarker in lung transplant recipients. Am J Respir Crit Care Med. 2016;195(7):942–52.
20. Galbán CJ, Boes JL, Bule M, Kitko CL, Couriel DR, Johnson TD, et al. Parametric response mapping as an indicator of bronchiolitis obliterans syndrome after hematopoietic stem cell transplantation. Biol Blood Marrow Transpl. 2014;20(10):1592–8.
21. Legland D, Kiêu K, Devaux M-F, Measures on 2D and 3d binary images. Image Anal Stereology. 2007;26(2):83–92.
22. Ram S, Pal R, Kumar M, Bell AJ, Wang JM, Labaki WW et al. Dictionary learning to predict COPD progression using topological PRM. C29 More than meets the eye: Advanced lung imaging. American thoracic society international conference abstracts: American Thoracic Society; 2023. p. A4717-A.
23. Ram S, Rodríguez JJ, editors. Single image super-resolution using dictionary-based local regression. 2014 Southwest Symposium on Image Analysis and Interpretation; 2014 6–8 April 2014.
24. Ram S, Rodriguez JJ, editors. Image super-resolution using graph regularized block sparse representation. 2016 IEEE Southwest Symposium on Image Analysis and Interpretation (SSIAI); 2016 6–8 March 2016.
25. Ram S. Sparse representations and nonlinear image processing for inverse imaging solutions. The University of Arizona; 2017.
26. Wang JM, Labaki WW, Murray S, Martinez FJ, Curtis JL, Hoffman EA, et al. Machine learning for screening of at-risk, mild and moderate COPD patients at risk of FEV(1) decline: Results from COPDGene and SPIROMICS. Front Physiol. 2023;14:1144192.
27. Ram S, Hoff BA, Bell AJ, Galban S, Fortuna AB, Weinheimer O, et al. Improved detection of air trapping on expiratory computed tomography using deep learning. PLoS ONE. 2021;16(3):e0248902.
28. Ram S, Reynolds L, Fortuna AB, Galban S, Vummidi DR, Kazerooni EA et al. Identification of expiratory air trapping in thoracic computed tomography using deep learning. A108 Pathophysiology in diffuse parenchymal lung diseases. American thoracic society international conference abstracts: American Thoracic Society; 2019. p. A2565-A.
29. Ding C, Peng H. Minimum redundancy feature selection from microarray gene expression data. J Bioinform Comput Biol. 2005;3(2):185–205.
30. Long F, Peng H, Ding C. Feature selection based on mutual information: Criteria of max-dependency, max-relevance, and min-redundancy. IEEE Trans Pattern Anal Mach Intell. 2005;27(08):1226–38.
31. Darbellay GA, Vajda I. Estimation of the information by an adaptive partitioning of the observation space. IEEE Trans Inf Theory. 1999;45(4):1315–21.
32. Ram S, Tang W, Bell AJ, Pal R, Spencer C, Buschhaus A, et al. Lung cancer lesion detection in histopathology images using graph-based sparse PCA network. Neoplasia. 2023;42:100911.
33. Ram S, Tang W, Bell AJ, Spencer C, Buschhuas A, Hatt CR, et al. Abstract PO-086: detection of cancer lesions in histopathological lung images using a sparse PCA network. Clin Cancer Res. 2021;27(5Supplement):PO–086.
34. Bhatt SP, Bodduluri S, Hoffman EA, John D, Newell J, Sieren JC, Dransfield MT, et al. Computed tomography measure of lung at risk and lung function decline in chronic obstructive pulmonary disease. Am J Respir Crit Care Med. 2017;196(5):569–76.
35. Boes JL, Bule M, Hoff BA, Chamberlain R, Lynch DA, Stojanovska J, et al. The impact of sources of variability on parametric response mapping of lung CT scans. Tomography. 2015;1(1):69–77.

Publisher's Note